PAPER • OPEN ACCESS

Numerical modelling of porosity with combined gas and shrinkage effects in HPDC

To cite this article: U Godwal *et al* 2023 *IOP Conf. Ser.: Mater. Sci. Eng.* **1274** 012028

View the article online for updates and enhancements.

Numerical modelling of porosity with combined gas and shrinkage effects in HPDC

U Godwal[1], S Bhagavath[1], B Ghaffari[2], M Li[2], P D Lee[3, 4] and S Karagadde[1*]

[1]Department of Mechanical Engineering, Indian Institute of Technology Bombay, Mumbai, 400076, India

[2]Ford Research and Advanced Engineering, Dearborn, USA

[3]Univeristy College London, WC1E 6BT, UK

[4]Research Complex at Harwell, Harwell Campus, OX11 0FA, UK

[*]Corresponding author: s.karagadde@iitb.ac.in

Abstract. High-pressure die casting is a manufacturing process in which near-net-shape components are produced rapidly under a pressurized environment. However, due to the relatively higher cooling rate prevailing during the process, isolated liquid pockets form at certain locations, leading to increased porosity formation. A one-dimensional deformable grid numerical model has been developed for predicting the evolution of a single pore in an elementary volume, which combines the diffusion model with the shrinkage affected growth. The model accounts for the change in pore size due to shrinkage and inter-granular growth. This model can provide predictions in representative volumes and be used for component level predictions by combining with a macroscopic model.

1. Introduction

High-pressure die casting (HPDC) is a popular casting process used to manufacture near-net shape components at a high production rate with a good surface finish, making it a desirable choice for manufacturing automotive parts [1]. However, HPDC components are also prone to defects, such as porosity and shear bands [2]. Due to the high pressures employed in HPDC, the interdendritic liquid metal feeding during solidification is better than in low-pressure or gravity casting. However, due to high cooling rates, the thin regions solidify early and might block the applied pressure (termed intensification when performed after filling) from reaching certain locations [3]. These isolated liquid pockets also suffer from the lack of liquid metal compensation during the later stages of solidification, leading to shrinkage porosity formation. Thus, isolated pockets can be subjected to a large range of pressure values, especially if an intensification stage is utilized, and it is important to estimate the resulting porosity level. Further, the shrinkage effects augment the diffusion-driven pore growth, leading to the unexpected presence of larger porosity compared to other regions [4]. Although several studies have modelled porosity in the past [5,6], the role of pressure and above combined effects remain largely unexplored.

In this study, we present a one-dimensional deforming grid numerical model to predict combined gas and shrinkage pore growth with different controlling parameters such as initial hydrogen concentration, pressure, and cooling rate. The growth of porosity into the interdendritic regions is also incorporated in the model.

2. Model Theory

For simulating the porosity formation in isolated liquid pockets undergoing different pressures, the combined gas and shrinkage porosity with high-pressure effects were considered. Initially, pure gas pore growth was modelled and verified with the literature. A 1D diffusion-controlled model was used to simulate the growth of an isolated pore [7], with the domain boundary representing an advancing solidification front. For pure gas pore growth, the diffusion equation was solved with the source term for hydrogen representing hydrogen partitioning during solidification. As shown in figure 1(a), the hydrogen influx, due to concentration gradient across a representative elementary volume (REV), drives the pore growth. A nucleated pore with an initial radius of 10 μm within an REV with a radius of 100 μm was considered with an initial hydrogen concentration uniformly distributed in the liquid metal.

The diffusion of hydrogen in the REV, is modelled using the species conservation equation in the liquid phase. The second term in the right-hand side of equation 1 is the source term, which accounts for the hydrogen rejection from the solid due to solubility difference during solidification [6].

$$\frac{\partial C_l}{\partial t} + \nabla.(uC_l) = \nabla.(D_l\nabla C_l) + (1-k)\frac{d(C_l f_s)}{dt} \qquad (1)$$

where, k is the hydrogen partition coefficient, C_l is the hydrogen concentration in the liquid, D_l is the diffusion coefficient, f_s is the solid fraction and u is the convective velocity.

2.1 Pore growth

The pore was considered to be surrounded by the liquid metal supersaturated by hydrogen [6,8,9]. A concentration gradient is developed due to low hydrogen content at the pore-liquid interface and higher amount of hydrogen at the solid-liquid interface (solid rejection). This eventually initiated the hydrogen influx into the pore. The pore pressure was given by the Young-Laplace equation [6,10,11]. The equation to determine the concentration at the pore-liquid interface was taken from Lee & Hunt [12] and Pequet et al. [13], which was governed by Sievert's law given as follows.

$$C_{lp} = S_l\sqrt{\frac{P_P}{P_l}} \qquad (2)$$

where, C_{lp} is the hydrogen concentration at the pore-liquid interface, S_l is Sievert's constant, P_P is the pore pressure and P_l is the liquid metal pressure. The concentration inside the pore was calculated using the ideal gas law.

The pore growth is assumed to be dominated by hydrogen diffusion, and the pore growth velocity can be obtained by calculating the rate of increase of mass in the pore [6]. The rate of increase of mass is balanced by two phenomena:

(i) The rate of concentration influx by virtue of concentration gradient and diffusion of hydrogen into the pore; and

(ii) The rate of mass flow due to pore-liquid interface movement. This is represented in a global coordinate frame of reference taken from the centre of the pore. The mass at the interface is given by $(4\pi R^2) C_{lp}$. With the movement of pore-liquid interface, the mass flow would be given by the second term on RHS in equation 3.

$$4\pi R^2 C_P \frac{dR}{dt} + \frac{4}{3}\pi R^3 \frac{dC_P}{dR}\frac{dR}{dt} = 4\pi R^2 D_l \frac{\partial C_l}{\partial r} + 4\pi R^2 C_{lp}\frac{dR}{dt} \qquad (3)$$

where, C_p is the concentration in the pore and R is the instantaneous pore radius. The left-hand side of equation 3 represents the increase in mass of the pore, and the right-hand side is composed of the rate of concentration influx and the rate of mass flow due to pore-liquid interface movement. Since the concentration at the pore-liquid interface is assumed to be at equilibrium, we can explicitly add the

local pressure term in equation 3. Also, it is appropriate to carry with the C_{lp} as it includes the local pressure governed by Sievert's law (equation 2). Simplifying the above equation provides the instantaneous pore interface velocity:

$$V_{inst}^P = \frac{1}{C_P - C_{lp} - C_d} D_l \left. \frac{\partial C_l}{\partial r} \right|_{r=R} \tag{4}$$

where C_d is given as:

$$C_d = -\frac{R}{3} \frac{dC_P}{dR} = \frac{2\sigma C_C}{(3R_G T)R} \tag{5}$$

where R_G is the universal gas constant and C_C is the conversion factor for relating number of moles per unit volume of hydrogen in terms of ml/100 gm of aluminium [6]. The equations are only solved in the liquid region, which reduces in volume as the solidification proceeds. It is assumed that the solid is permeable, and the liquid is pushed away from the domain during pore growth. The pore-liquid interface will move as the pore growth is incorporated due to hydrogen influx into the pore. A deformable grid approach ensures that at each time step, a node is present at the moving boundary [14]. A fixed number of nodes (100 nodes) are considered with the shrinking grid.

Pore growth is captured by solving the species equation, calculating the hydrogen influx and tracking the pore-liquid interface. The code was also extended to the solid and pore growth simultaneously. The boundary movement of the solid is also captured, and the liquid region shrinks between the pore and solid. A constant velocity is assumed with linear movement in the radial direction for solid boundary movement.
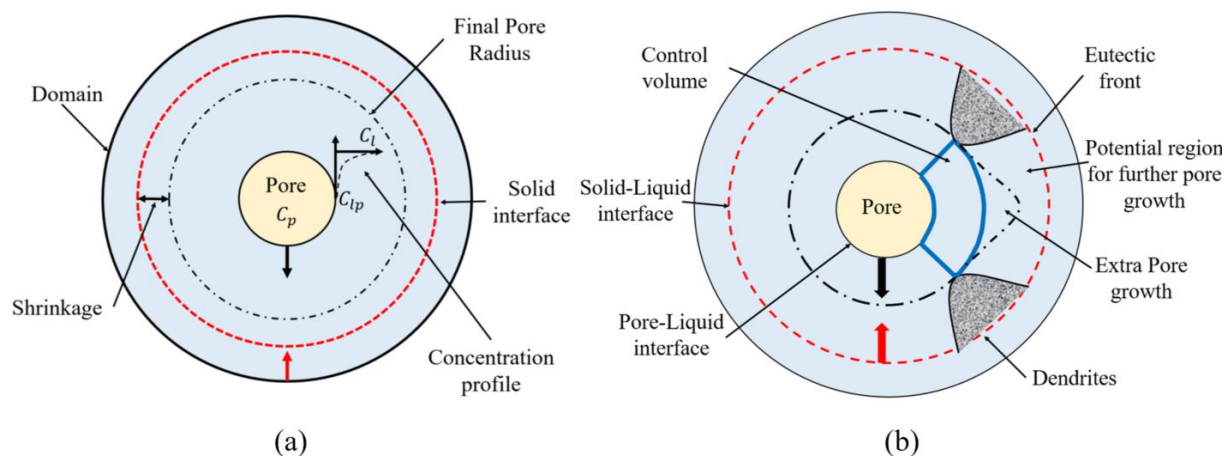
Figure 1. (a) Schematic considered for 1D diffusion model and addition of shrinkage effect, (b) Schematic of restricted pore growth

2.2 Restricted gas pore growth

A gas pore grows as a sphere until it encounters a restriction, as shown in figure 1(b). Once the pore impinges on a growing dendrite, the spherical growth of a pore is terminated, and the further growth as a perturbation out of a spherical surface is initiated [10–12]. The solid-liquid interface was tracked simultaneously with the pore-liquid interface to capture the pore-solid interaction.

The perturbation after the pore-solid interaction is modelled using the approximation as a spherical cap, and the radius for the spherical cap is adopted from Atwood et al. [10]:

$$R_C = \sqrt{R_G^2 - (z - R_G)^2} - R_G \qquad (6)$$

where, R_G is the radius of the solid grain impinging the pore, R_C is the radius of the spherical cap, and z is the growth length. After the pore-solid interaction starts, the pore usually adopts the 3-D negative shape of the solid [15]. The curvature effects also enhance the pore growth, but these effects are not included in this study.

2.3 Combined gas-shrinkage effects

During solidification, after the dendritic coherency is reached [16,17], the feeding is restricted due to the poor permeability of the mush. In this work, the shrinkage effects are combined with the gas effects to obtain an updated pore evolution when shrinkage effects exist. An instantaneous shrinkage volume is calculated, which is added once the gas pore is fully grown. The total radius is calculated after adding the shrinkage effects.

It is assumed that there is no liquid feeding to compensate for the shrinkage effects after the dendritic coherency is reached [1], and the control volume is treated as an isolated pocket which forms during HPDC. After entrapment of gas pore due to coherency, the metal flow for volumetric shrinkage compensation is restricted, and hence shrinkage effects enhance the pore radius. The gas pore becomes the nucleation point for the micro-shrinkage formation. The above points can be well understood by the pressure balance and the effect of shrinkage pressure for enhancing the pore size [17,18].

## 3. Results and discussion

3.1 Hydrogen concentration

Pore growth and final pore radius are captured for different initial hydrogen concentrations, as shown in figure 2. The results are quantified, and the trend matches well with the literature [10–12] (see figure 2(a)). For validating with the Lee & Hunt model [12], all the boundary conditions were kept the same with a grid spacing of 200 μm and a time step of 25 ms. The error is found to be less than 10% at all hydrogen content. The 10% error is due to difference in capturing the pore growth in both models in spite of considering same hydrogen content. The present model was extended for higher hydrogen content. The concentration gradient was high for higher hydrogen concentration, resulting in faster growth. With increasing the initial hydrogen concentration from 1 to 5 ml/100 g of Al, an increment from 30 μm to 63 μm (i.e. twice) of final pore radius is reported (see figure 2(b)).

3.2 Pressure

Radius-pressure trends were observed from the 1D diffusion code for high pressure values. All other parameters were kept constant, and only pressure values were changed. The initial hydrogen content was taken as 2 ml/100 gm of Al for all cases. A reduction of 50% was observed for the final pore radius, for increasing the pressure from 1 to 50 atm (see figure 2(b)). Specific experimental data for isolated gas pores at higher pressures are not available in literature, to the best of the author's knowledge. In-situ experiments capturing the isolated gas pores at higher pressures will be carried out to validate the numerical model. However, a similar decreasing trend with pressure was observed by C. Wang et al. [19]. According to the governing physics, the external pressure restricts the pore growth and the radius variation is expected to flatten at higher pressure, which can be observed in figure 2(b). Due to the higher cooling rate and faster solidification in HPDC, the time for hydrogen diffusion is less, and hence the pore is smaller in size than other casting processes. Although solidification rate was used in this case, it should be noted that many other effects, such as dilatancy effects, can also affect pore growth during high pressure die casting.
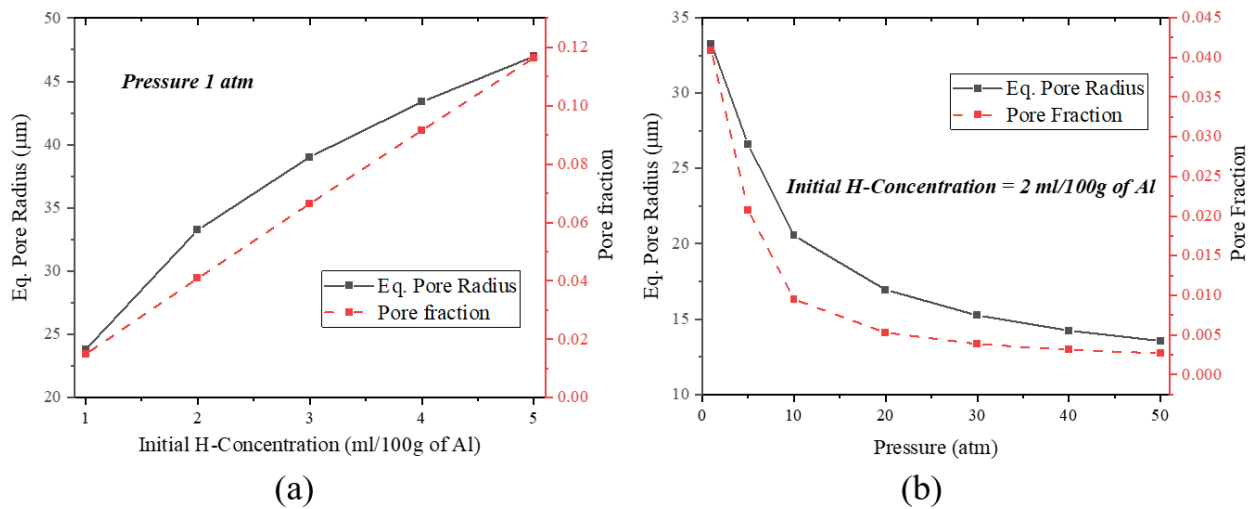
3.3 Restricted gas pore growth

Predictions of the model for pore fraction and equivalent pore radius are plotted in figure 3(a) for different initial hydrogen concentrations, showing a near-linear variation. The pore-liquid and solid-liquid interface movements were tracked until their interaction. The same trend for radius variation with hydrogen content has been observed in literature [10,20]. The pressure was kept constant at 1 atm. The equivalent pore radius increased by 50%, for the initial hydrogen content varying from 1 to 5 ml/100g of Al.
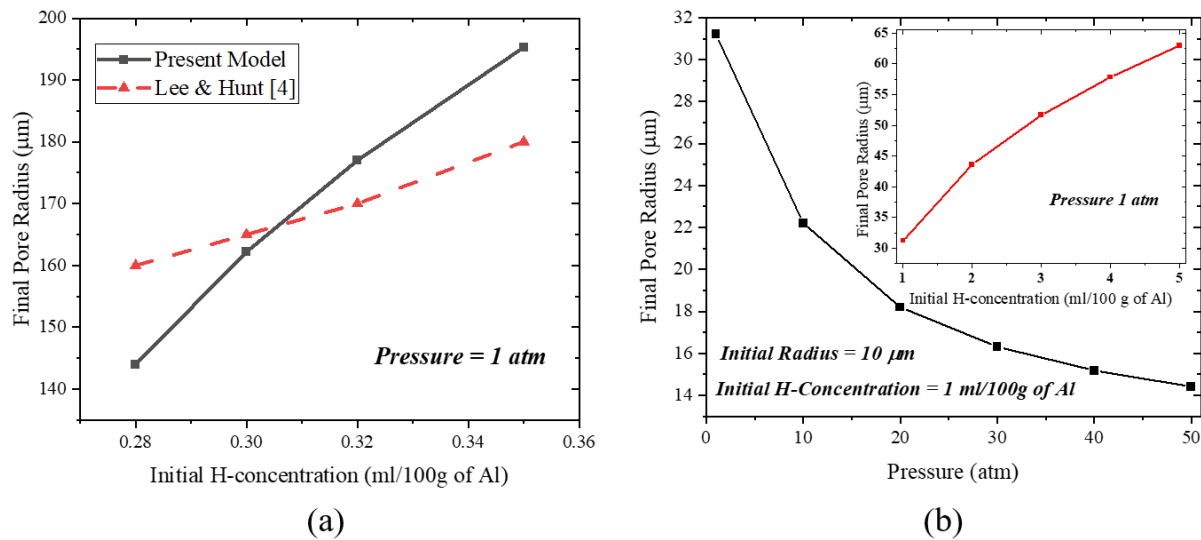
Figure 2. (a) Final pore radius with initial hydrogen content (validation case grid spacing 200 μm and time step as 25 ms with initial hydrogen content as 0.28, 0.30, 0.32 and 0.35 ml/100 gm Al), and (b) Final pore radius variation with pressure and initial hydrogen content for initial pore radius as 10 μm and domain size of 100 μm (present model)

The final pore radius and pore fraction variation with the pressure is also plotted. Figure 3(b) shows the decreasing trend for final pore radius and pore fraction with increased pressure. As the pressure is increased from 1 to 50 atm, the final pore radius showed a decrement from 33 μm to 14 μm.

Figure 3. Restricted pore growth (a) Eq. Pore radius and pore fraction variation with Hydrogen concentration and (b) Eq. pore radius and pore fraction variation with pressure

3.4 Combined gas and shrinkage effects

The porosity formed in isolated liquid pockets in HPDC is affected by both gas concentration and shrinkage. The shrinkage effects enhance the pore growth, and hence the combined gas and shrinkage pores are bigger in size than the pure gas pores. Initially, the pore grows purely due to hydrogen diffusion, but at later stages of solidification shrinkage-driven effects dominate the pore growth (see figure 4(a)).

The final pore radius with varying initial hydrogen content for pure gas and combined gas and shrinkage effects, displaying an increase with higher hydrogen concentration is shown in figure 4(a). For higher hydrogen content, the difference in the pure gas and combined gas and shrinkage pore is reduced due to the smaller amount of liquid metal present in REV, eventually having less shrinkage. An increment of 33% of pore radius was observed at 1 ml/100g of Al, which decreased to 11% increment at 5 ml/100g of Al, depicting less contribution of shrinkage effect at higher H-content.

Figure 4(b) shows the final pore radius variation with pressure for pure gas and combined effects. At high pressure values, the contribution of shrinkage effect is larger than the contribution from the gas content, compared to lower pressure values [21]. At low pressure values, the increment in the combined gas and shrinkage pore radius is 25%. At a higher pressure value, the increment is 61%, which depicts the more significant contribution of shrinkage porosity at higher pressures.
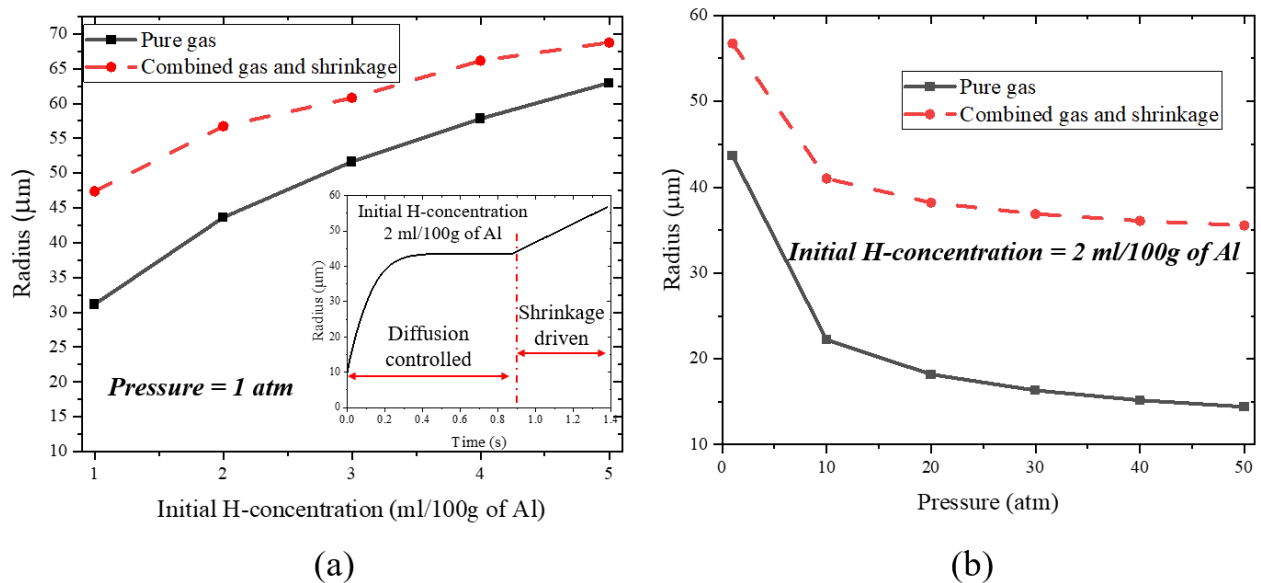
Figure 4. Combined gas and shrinkage pore growth (a) Final pore radius variation with initial hydrogen concentration and (b) Final pore radius variation with pressure

4. Conclusions

The growth of porosity in HPDC due to combined gas and shrinkage effects was studied with respect to different process parameters and its growth with different varying parameters was studied. A one-dimensional diffusion-driven numerical model was used for estimating the gas pore growth. The variation of pore radius with pressure and hydrogen concentration levels was studied. The model established the expected reduction in pore radius with pressure. More importantly, the quantitative extent of reduction with the applied pressure was successfully captured. The shrinkage was found to have a considerable influence on the final porosity (gas and shrinkage) at higher pressure values. The methodology provides porosity estimates for all ranges of pressure and hydrogen level that represent the local variation in a typical HPDC casting. The model is expected to help in making macroscopic predictions of porosity in HPDC components, aiding in locating probable defect locations.

Acknowledgments

5. References

[1]   Otarawanna S, Laukli H I, Gourlay C M and Dahle A K 2010 Feeding mechanisms in high-pressure die castings *Metall. Mater. Trans. A Phys. Metall. Mater. Sci.* **41** 1836–46

[2]   Dahle A K and StJohn D H 1998 Rheological behaviour of the mushy zone and its effect on the formation of casting defects during solidification *Acta Mater.* **47** 31–41

[3]   Bhagavath S, Gong Z, Wigger T, Shah S, Ghaffari B, Li M, Marathe S, Lee P D, Karagadde S, Gong Z, Wigger T, Shah S, Ghaffari B, Li M, Marathe S, Lee P D and Karagadde S 2021 Role of the local stress systems on microstructural inhomogeneity during semisolid injection

[4]   Lee S G and Gokhale A M 2006 Formation of gas induced shrinkage porosity in Mg-alloy high-pressure die-castings *Scr. Mater.* **55** 387–90

[5]   Lee P D, Chirazi A and See D 2001 Modeling microporosity in aluminum-silicon alloys: A review *J. Light Met.* **1** 15–30

[6]   Karagadde S and Dutta P 2016 A comparison of time-scales governing the interaction and growth of hydrogen bubbles with a solidifying front *Int. Commun. Heat Mass Transf.* **79** 16–20

[7]   Yu W, Ma C, Ma Y and Xiong S 2021 Correlation of 3D defect-band morphologies and mechanical properties in high pressure die casting magnesium alloy *J. Mater. Process. Technol.* **288** 116853

[8]   Bhagavath S, Cai B, Atwood R, Li M, Ghaffari B, Lee P D and Karagadde S 2019 Combined Deformation and Solidification-Driven Porosity Formation in Aluminum Alloys *Metall. Mater. Trans. A Phys. Metall. Mater. Sci.* **50** 4891–9

[9]   Karagadde S, Sundarraj S and Dutta P 2012 A model for growth and engulfment of gas microporosity during aluminum alloy solidification process *Comput. Mater. Sci.* **65** 383–94

[10]   Atwood R C, Sridhar S, Zhang W and Lee P D 2000 Diffusion-controlled growth of hydrogen pores in aluminium-silicon castings: In situ observation and modelling *Acta Mater.* **48** 405–17

[11]   Atwood R C and Lee P D 2002 A three-phase model of hydrogen pore formation during the equiaxed dendritic solidification of aluminum-silicon alloys *Metall. Mater. Trans. B Process Metall. Mater. Process. Sci.* **33** 209–21

[12]   Lee P D and Hunt J D 2001 Hydrogen porosity in directionally solidified aluminium-copper alloys: A mathematical model *Acta Mater.* **49** 1383–98

[13]   Pequet C, Rappaz M and Gremaud M 2002 Modeling of microporosity, macroporosity, and pipe-shrinkage formation during the solidification of alloys using a mushy-zone refinement method: Applications to aluminum alloys *Metall. Mater. Trans. A Phys. Metall. Mater. Sci.* **33** 2095–106

[14]   Voller V R, Boundary M and Notes P Chapter 6 Deforming Grid Solutions of the Stefan Problem 1–35

[15]   Felberbaum M and Rappaz M 2011 Curvature of micropores in Al-Cu alloys: An X-ray tomography study *Acta Mater.* **59** 6849–60

[16]   Kubo K and Pehlke R D 1985 Mathematical modeling of porosity formation in solidification *Metall. Trans. B* **16** 359–66

[17]   Stefanescu D M 2005 Computer simulation of shrinkage related defects in metal castings - A review *Int. J. Cast Met. Res.* **18** 129–43

[18]   Gu C, Ridgeway C D, Cinkilic E, Lu Y and Luo A A 2020 Predicting gas and shrinkage porosity in solidification microstructure: A coupled three-dimensional cellular automaton model *J. Mater. Sci. Technol.* **49** 91–105

[19]   Wang C tao, Yao J, Zhao H dong and Yang R sheng 2019 Influence of intensification pressures on pores in die-cast ADC12 alloys *China Foundry* **16** 184–9

[20]   Atwood R C and Lee P D 2003 Simulation of the three-dimensional morphology of solidification porosity in an aluminium-silicon alloy *Acta Mater.* **51** 5447–66

[21]   Zhang Y, Lordan E, Dou K, Wang S and Fan Z 2020 Influence of porosity characteristics on the variability in mechanical properties of high pressure die casting (HPDC) AlSi7MgMn alloys *J. Manuf. Process.* **56** 500–9